

Iontronic neuromorphic signalling with conical microfluidic memristors

T. M. Kamsma,^{1,2} W. Q. Boon,¹ T. ter Rele,^{1,3} C. Spitoni,² and R. van Roij¹

¹*Institute for Theoretical Physics, Utrecht University, Princetonplein 5, 3584 CC Utrecht, The Netherlands*

²*Mathematical Institute, Utrecht University, Budapestlaan 6, 3584 CD Utrecht, The Netherlands*

³*Soft Condensed Matter, Debye Institute for Nanomaterials Science, Utrecht University, Princetonplein 1, 3584 CC Utrecht, The Netherlands*

(Dated: June 28, 2023)

Experiments have shown that the conductance of conical channels, filled with an aqueous electrolyte, can strongly depend on the history of the applied voltage. These channels hence have a memory and are promising elements in brain-inspired (iontronic) circuits. We show here that the memory of such channels stems from transient concentration polarization over the ionic diffusion time. We derive an analytic approximation for these dynamics which shows good agreement with full finite-element calculations. Using our analytic approximation, we propose an experimentally realisable Hodgkin-Huxley iontronic circuit where micrometer cones take on the role of sodium and potassium channels. Our proposed circuit exhibits key features of neuronal communication such as all-or-none action potentials upon a pulse stimulus and a spike train upon a sustained stimulus.

Transport phenomena of charged species through channels in the nanometre and micrometre regime play a key role in a plethora of applications [1–12]. An exciting emerging direction of research is that of iontronics, the use of ion transport for signalling [13], which holds the promise of interfacing with biological systems [13–16] and processing information via multiple signal carriers and chemical regulation [17, 18]. In particular conical channels have garnered significant interest for such applications [14, 15, 19–23], as they exhibit current rectification thereby acting as ionic diodes [9, 19, 24–26]. This has been extensively studied experimentally [19, 22, 27–31] as well as numerically [23, 32–35] and several analytic descriptions are available [25, 36–38]. Due to this interest cones are now comparatively easy to fabricate [39–42]. Recently, it has been observed that the conductance of cones exhibits hysteresis when driven by an alternating potential [43–53], and hence they are memristors (resistors with memory) [54–57]. Various explanations of this effect have been explored [43–48], the most recent hypothesis being dynamic concentration polarization [50–53], which we confirm below. Memristors in general are essential components for neuromorphic (brain-inspired) circuits, since much of their dynamics is analogous to the synapses that connect neurons [58–62] and to the ion channels responsible for electric signaling within neurons [58, 63]. The popularity of memristors and neuromorphic circuits has drastically increased [64–66] due to the prospects of energy-efficient computers [67–69] and bio-compatibility [59, 70–74]. Solid-state devices received the majority of attention [64–66, 68], while the brain in contrast relies on ion transport in an aqueous medium [75, 76]. Iontronic circuits, based on the same signalling medium as the brain, sparked recent interest as a promising platform for a new generation of (neuromorphic) computing devices [17, 77–80]. However, the development of neuromorphic iontronic devices is still in its infancy [13, 79] and a deeper understanding of underlying mechanisms and possible end-uses is needed [79, 80].

In this Letter we propose a neuromorphic iontronic circuit where all-or-none action potentials [75, 76, 81] and neuronal spiking [76, 82–85] are obtained through micrometer cones

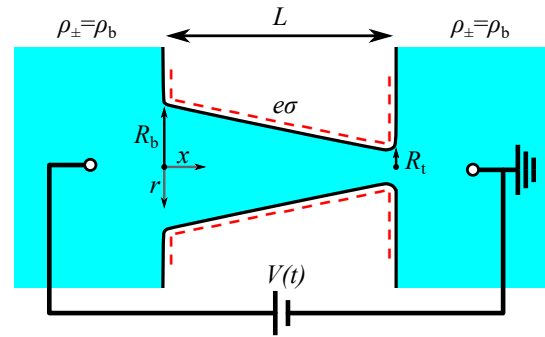


FIG. 1. Schematic representation of an azimuthally symmetric conical channel of length L , base radius R_b , and tip radius $R_t < R_b$, connecting two bulk reservoirs of a 1:1 aqueous electrolyte, with bulk concentrations ρ_b . The channel wall carries a surface charge density $e\sigma$. An AC electric potential drop $V(t)$ over the channel drives an ionic charge current $I(V(t), t) = g(V(t), t)V(t)$ with $g(V(t), t)$ the channel conductance. The AC potential causes transient concentration polarisation resulting in a volatile conductance memory.

filled with aqueous electrolyte. First we solve for the dynamic competition between ionic diffusion, conduction and advection, using the Poisson-Nernst-Planck-Stokes equations and the steady-state results in Ref. [25]. We obtain a differential equation with no free parameters describing transient concentration polarization and we surprisingly find that the inhomogeneous conduction responsible for concentration polarization retains memory over slow (diffusive) timescales. Using this result we construct an experimentally accessible iontronic circuit of several cones, batteries, and a capacitor and show that the time-dependent voltage over this circuit exhibits multiple key features of neuronal communication. While neuronal behaviour in the form of an emerging voltage spike train has been reported in a simulated iontronic circuit containing quasi two-dimensional nanochannels that connect aqueous electrolytes [86], the defining all-or-none law of action potentials [75, 76, 81], a phenomenon considered to be a requirement for artificial neurons [66], has not yet been reported. Furthermore the circuit in Ref. [86] requires comparatively difficult to fabricate two-dimensional channels and

Nernst potentials that do not directly affect the circuit voltage, complicating experimental accessibility. In this Letter we overcome these issues. As conical pores are a well-known iontronic model system, we believe our proposed neuromorphic circuit is within experimental reach.

We first consider a single conical channel, schematically illustrated in Fig. 1, that connects two bulk reservoirs of an incompressible aqueous 1:1 electrolyte with viscosity $\eta = 1.01 \text{ mPa} \cdot \text{s}$, mass density $\rho_m = 10^3 \text{ kg} \cdot \text{m}^{-3}$ and electric permittivity $\epsilon = 0.71 \text{ nF} \cdot \text{m}^{-1}$, containing ions with diffusion coefficients $D_{\pm} = D = 1.75 \text{ } \mu\text{m}^2 \text{ms}^{-1}$ and charge $\pm e$ with e the proton charge. At the far side of both reservoirs we impose a fixed pressure $P = P_0$ and fixed ion concentrations $\rho_{\pm} = \rho_b = 0.1 \text{ mM}$. The reservoirs are connected by an azimuthally symmetric conical channel with base radius $R_b = 200 \text{ nm}$ at $x = 0$ and tip radius $R_t = R_b - \Delta R = 50 \text{ nm}$ at $x = L \gg R_b$, the central axis being at radial coordinate $r = 0$. Unless otherwise stated the channel has length $L = 10 \text{ } \mu\text{m}$, hence the geometry is similar to cones in Ref. [39]. The channel radius is described by $R(x) = R_b - x\Delta R/L$ for $x \in [0, L]$. We assume a uniform surface charge density $e\sigma = -0.0015 \text{ enm}^{-2}$ on the channel walls, resulting in a surface potential $\psi_0 \approx -10 \text{ mV}$ (typical for PMMA [87]) and an electric double layer that screens the surface charge with Debye length $\lambda_D \approx 30 \text{ nm}$. On the far side of the reservoir connected to the base we impose an electric potential $V(t)$, while the far side of the other reservoir is grounded, which leads to an electric potential profile $\Psi(x, r, t)$, an electro-osmotic fluid flow with velocity field $\mathbf{u}(x, r, t)$ and ionic fluxes $\mathbf{j}_{\pm}(x, r, t)$ with $\mathbf{j}_+ - \mathbf{j}_-$ the charge flux. A relatively low surface potential ψ_0 ensures a weak electro-osmotic flow $Q(V)$, allowing conductance tuning over a wider voltage range [25, 49, 88]. We have $Q(V)/V = -\pi R_t R_b \epsilon \psi_0 / (\eta L) \approx 22.7 \text{ } \mu\text{m}^3 \text{s}^{-1} \text{V}^{-1}$ for our standard parameter set [25].

Transport through the conical channel is described by the Poisson-Nernst-Planck-Stokes (PNPS) Eqs. (1)-(4) given by

$$\nabla^2 \Psi = -\frac{e}{\epsilon}(\rho_+ - \rho_-), \quad (1)$$

$$\frac{\partial \rho_{\pm}}{\partial t} + \nabla \cdot \mathbf{j}_{\pm} = 0, \quad (2)$$

$$\mathbf{j}_{\pm} = -D_{\pm} \left(\nabla \rho_{\pm} \pm \rho_{\pm} \frac{e \nabla \Psi}{k_B T} \right) + \mathbf{u} \rho_{\pm}, \quad (3)$$

$$\rho_m \frac{\partial \mathbf{u}}{\partial t} = \eta \nabla^2 \mathbf{u} - \nabla P - e(\rho_+ - \rho_-) \nabla \Psi; \quad \nabla \cdot \mathbf{u} = 0. \quad (4)$$

Here electrostatics is accounted for by the Poisson Eq. (1), the conservation of ions by the continuity Eq. (2), the combination of Fickian diffusion, Ohmic conduction, and Stokesian advection by the Nernst-Planck Eq. (3), and finally the force balance on the (incompressible) fluid by the Stokes Eq. (4). This system is closed upon imposing no-slip and blocking boundary conditions on the channel wall, $\mathbf{u} = 0$ and $\mathbf{n} \cdot \mathbf{j}_{\pm} = 0$, respectively, together with Gauss' law $\mathbf{n} \cdot \nabla \Psi = -e\sigma/\epsilon$, with \mathbf{n} the wall's inward normal vector.

When an electric potential $V(t)$ is applied, the ionic concentrations $\rho_{\pm}(x, r, t)$ will deviate from their equilibrium profiles, thereby changing the channel conductance [25]. In Ref. [25] the stationary state version of the PNPS equations (1)-(4) is solved for a static potential V , which gives rise to the sta-

tionary charge current $I = g_{\infty}(V)V$, where the static conductivity $g_{\infty}(V)$ was found to be governed by the (voltage-dependent) radially averaged salt concentration $\bar{\rho}_s(x, V) = 2 \int_0^{R(x)} r \rho_s(x, V, r) dr / R(x)^2$, with $\rho_s = \rho_+ + \rho_-$ (see Supplemental Material for full expression). For small potentials $e|V|/k_B T \ll |w|(R_b/R_t)$, with $w = eD\eta/(k_B T \epsilon \psi_0) \simeq -9.5$ the ratio of ionic to electro-osmotic mobility [88], the pore concentration equals the bulk concentration $\bar{\rho}_s(x, V) = 2\rho_b$, yielding $g_{\infty}(V) = g_0$, with the Ohmic cone conductance $g_0 = (\pi R_t R_b / L)(2\rho_b e^2 D / k_B T)$, and the resulting current follows Ohm's law $I = g_0 V$ [25]. For large static potential drops the cone exhibits diodic behaviour due to concentration polarisation, with the cone conductance determined by the salt concentration profiles according to

$$\begin{aligned} \frac{g_{\infty}(V)}{g_0} &= \int_0^L \bar{\rho}_s(x, V) dx / (2\rho_b L) \\ &= 1 + \Delta g \int_0^L \left[\frac{x}{L} \frac{R_t}{R(x)} - \frac{e^{\text{Pe}(V) \frac{x}{L} \frac{R_t^2}{R_b R(x)}} - 1}{e^{\text{Pe}(V) \frac{R_t}{R_b}} - 1} \right] dx / L, \end{aligned} \quad (5)$$

where an approximation is made compared to the more accurate dependence on $L/\int_0^L (\bar{\rho}_s(x, V))^{-1} dx$ to reduce computational complexity [25]. The static conductance $g_{\infty}(V)$ depends on V through the Péclet number at the narrow end $\text{Pe}(V) = Q(V)L/(D\pi R_t^2) = -(eV/k_B T)(R_b/R_t)w^{-1}$, where for our standard parameters $\text{Pe}(V)/V \approx 16.5 \text{ V}^{-1}$, and $\Delta g \equiv -2w(\Delta R/R_b)Du \approx -3.6$ with the tip Dukhin number $Du = \sigma/(2\rho_b R_t) \approx -0.25$. In our case of $\sigma < 0$, $V > 0$ depletes the channel of ions such that $g_{\infty}(V)/g_0 < 1$ whereas $V < 0$ results in ion accumulation such that $g_{\infty}(V)/g_0 > 1$, which is responsible for the static diode behaviour of the cone [25].

Voltage driven accumulation or depletion of ions from the pore is not instantaneous, as it takes time for the ions to move into or out of the channel. In the Supplemental Material (SM) [89] we derive from the PNPS equations (1)-(4) that the typical timescale for this process is not given by an RC-like time as suggested in Ref. [46], but rather by a diffusion-like time

$$\tau = \frac{L^2}{12D}, \quad (6)$$

which for our standard parameter set yields $\tau = 4.8 \text{ ms}$. To obtain an analytic approximation for the time-dependent conductance $g(V(t), t)$ we assume a single exponential relaxation of the salt-concentration with timescale τ towards the steady-state concentration profile. This natural approach has been successfully applied to investigate memristor dynamics before [78, 90] and is verified for conical channels in Fig. 2. Using Eq. (5), this approach yields the following expressions for the time-dependent conductance $g(V(t), t)$ and current $I(V(t), t)$

$$\frac{\partial g(V(t), t)}{\partial t} = \frac{g_{\infty}(V(t)) - g(V(t), t)}{\tau}, \quad (7)$$

$$I(V(t), t) = g(V(t), t)V(t). \quad (8)$$

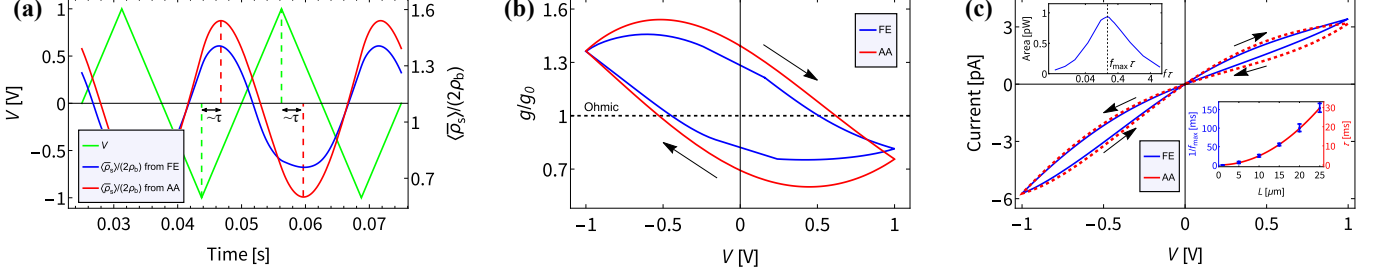


FIG. 2. Comparisons of finite-element calculations (FE, blue) of the full PNPS equations (1)-(4) and our analytic approximation Eqs. (5)-(8) (AA, red) when a periodic triangle potential $V(t)$ (green in (a)) with amplitudes ± 1 V and frequency $f = 40$ Hz is applied. In (a) we show two periods of the time-dependent laterally averaged salt concentration $\langle \bar{\rho}_s \rangle(V(t), t) \equiv \int_0^L \bar{\rho}_s(x, V(t), t) dx/L$, in (b) the corresponding conductance-voltage diagram as per Eqs. (5) and (7), and in (c) the corresponding current-voltage diagram with a clear pinched hysteresis loop. The left inset of (c) shows the dependence of the enclosed area in I-V hysteresis loop on the (dimensionless) triangle potential frequency $f\tau$ with a maximum at $f_{\max} \tau \approx 0.19$ for $L = 10 \mu\text{m}$. The right inset of (c) shows the dependence of $1/f_{\max}$ (blue) and of the characteristic time τ from Eq. (6) (red) on the channel length L , satisfying $f_{\max} \tau \approx 0.19$ for all L considered.

Eq. (7) shows that the conductance $g(V(t), t)$ depends on the entire timetrace of the potential $V(t)$. This conductance memory is the key feature of a memristor [57], in fact Eqs. (7) and (8) indeed fit the mathematical definition of a generic voltage-driven memristor [56–58]. From now on we will refer to Eqs. (5)-(8) as the approximate analytical (AA) solution of the PNPS equations [25]. To verify the AA we also numerically solve the full PNPS equations (1)-(4) in the geometry of a conical channel using the finite-element (FE) analysis package COMSOL [91, 92].

In Fig. 2(a) we compare the time-dependent laterally averaged salt concentrations $\langle \bar{\rho}_s \rangle(V(t), t) \equiv \int_0^L \bar{\rho}_s(x, V(t), t) dx/L$ from FE calculations (blue) and the AA (red), which for the AA is equivalent to $g(V(t), t)/g_0$. In both cases $V(t)$ is a periodic triangle potential (green) with amplitudes ± 1 V and a period of 25 ms. The features of the AA and FE calculations essentially agree, not only the typical amplitude of $\langle \bar{\rho}_s \rangle(V(t), t)$, but also the time lag $\sim \tau$ (Eq. (6)) between $V(t)$ and $\langle \bar{\rho}_s \rangle(V(t), t)$, as indicated by the two pairs of dashed vertical lines. This time lag results in a hysteretic conductance-voltage diagram, shown in Fig. 2(b). Here the AA and FE calculations agree with each other again, verifying the proposed relation of $\langle \bar{\rho}_s \rangle(V(t), t)$ with the conductance $g(V(t), t)$.

Translating the results of Fig. 2(b) to the current with Eq. (8) we obtain the current-voltage (I-V) plot of Fig. 2(c), which shows the memristor hallmark of a pinched hysteresis loop [56]. We again find agreement between the AA and FE calculations and the I-V loop resembles previously reported experimental results from comparable systems [43–45, 49, 52]. The shape of the hysteresis loop depends on the frequency f of the applied triangle potential $V(t)$. The enclosed area inside the loop shrinks to 0 for $f\tau \ll 1$ and $f\tau \gg 1$ and shows a maximum at $f_{\max} \tau \approx 0.19$ for the standard parameter set, as shown in the left inset of Fig. 2(c). In the right inset of Fig. 2(c) we see that the one-to-one relation $f_{\max} \tau \approx 0.19$ also holds for various lengths L , further supporting the validity of Eq. (6). Excitingly, the quadratic de-

pendence of τ on the channel length L offers strong control over the channel memory retention time, a desirable trait [61].

Having derived Eqs. (6)-(8) for the memristive effect in a single conical channel, we now turn our attention to modelling a brain-inspired iontronic circuit. Electric signalling within a neuron is facilitated by an action potential (AP), a propagating voltage spike over the cell membrane [75]. APs obey the all-or-none law, i.e. an AP either fails to initiate upon a subcritical stimulus or completely occurs for a supercritical stimulus, with no gradual transition in between [75, 76, 81], and can be sequentially generated, resulting in a spike train [76, 82–85]. These neuronal features of electric activity over the membrane have been successfully modelled by an equivalent circuit as in Fig. 3(a), first quantitatively characterised by Hodgkin and Huxley [93], which has formed an extensively used basis to mathematically model neuronal signalling [94–100]. Interestingly, the mathematical descriptions of the biological potassium and sodium channel conductances g_K and g_{Na} in the Hodgkin-Huxley (HH) model were later identified to be descriptions of memristors [63]. Therefore we expect similar spontaneous neuronal features by assembling conical channels in a HH-like circuit, where the micrometer channels take on the role of the potassium and sodium channels.

Inspired by HH circuits we present the circuit shown in Fig. 3(b). This circuit consists of a capacitor with capacitance $C = 5$ fF (corresponding to the typical capacitance of a biological neuronal membrane of area $\sim 1 \mu\text{m}^2$ [101]), connected in parallel with three oriented conical channels, with conductances g_+ , g_- and g_s and lengths $L_{\pm} = 1 \mu\text{m}$ and $L_s = 25 \mu\text{m}$. As per Eq. (6), the timescales $\tau_{\pm} \approx 0.048$ ms of the two fast channels are identical, while the timescale $\tau_s \approx 30$ ms $\gg \tau_{\pm}$ is much slower. The conical channels are connected in series to batteries with potentials $E_{\pm} = \pm 0.975$ V for the two fast channels and $E_s = -0.5$ V for the slow channel. The imposed stimulus current $I(t)$ is the control parameter and determines whether spiking occurs. The electric potential $V_m(t)$ over the circuit shown in Fig. 3(b) is equivalent to the membrane potential over a neuronal membrane [93].

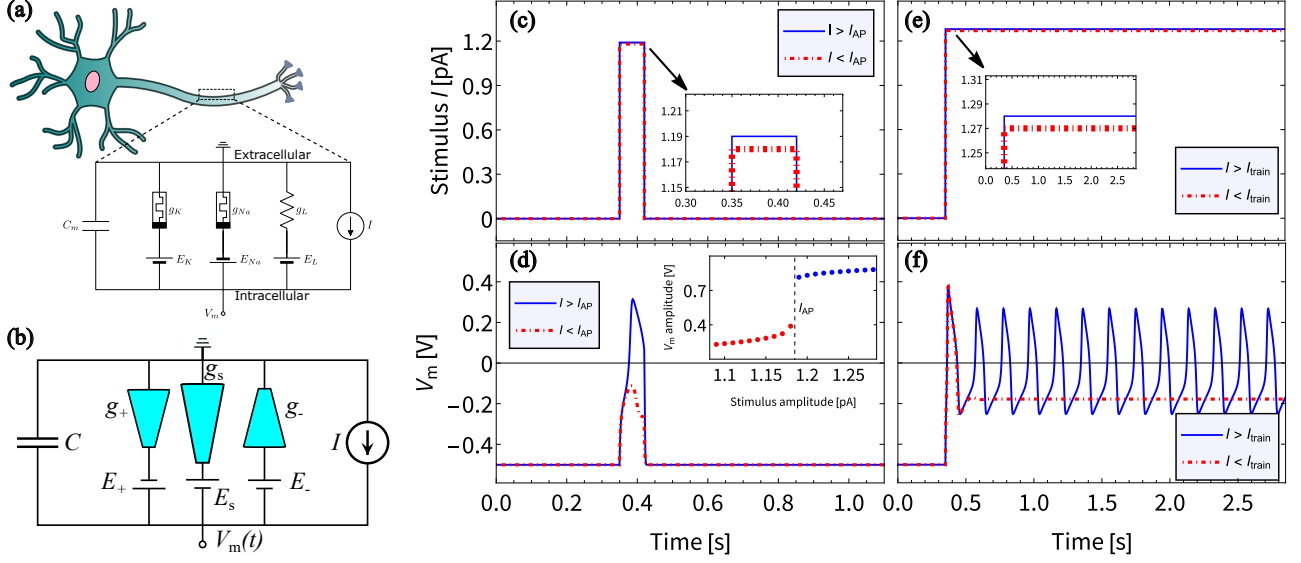


FIG. 3. (a) The Hodgkin-Huxley circuit model with Na^+ , K^+ and leak channels, a capacitor and batteries corresponding to the Na^+ and K^+ Nernst potentials [93]. (b) Schematic representation of our proposed circuit containing three oriented conical channels, connected in series to individual batteries and in parallel to a capacitor. The electric potential difference $V_m(t)$ over the capacitor can be driven by an imposed stimulus current $I(t)$. (c) The imposed subcritical (red) and supercritical (blue) current pulse $I(t)$, and (d) the resulting $V_m(t)$ from Eq. (9), displaying an all-or-none action potential, as can be seen by the jump in spike amplitude around I_{AP} as shown in the inset. (e) The imposed subcritical (red) and supercritical (blue) sustained currents $I(t)$, and (f) the resulting $V_m(t)$, where a spike train emerges for $I(t) > I_{\text{train}}$.

Invoking Kirchoff's law, the potential $V_m(t)$ will evolve according to

$$C \frac{dV_m(t)}{dt} = I(t) - \sum_{i \in \{+, -, s\}} g_i(V_i(t), t) (V_m(t) - E_i), \quad (9)$$

where the conductances $g_i(V_i(t), t)$, determined by their individual laterally averaged salt concentrations as per Eq. (5), each evolve according to Eq. (7), however with arguments V_i of $g_{i,\infty}(V_i)$ given by $V_-(t) = V_m(t) - E_-$, $V_+(t) = -V_m(t) + E_+$ and $V_s(t) = -V_m(t) + E_s$. The differences in signs of the potentials reflect the different orientations of the channels as depicted in Fig. 3(b). Eqs. (6), (7) and (9) form a closed set of equations, which we numerically solve with initial conditions $V(0) = -0.5$ V and $g_i(V_i(0), 0) = g_{0,i}$.

Fig. 3(c) shows a subcritical pulse current $I < I_{\text{AP}}$ (red) and supercritical pulse current $I > I_{\text{AP}}$ (blue), both of duration 70 ms, and Fig. 3(d) shows the two resulting membrane potentials $V_m(t)$. For the supercritical stimulus $V_m(t)$ fully depolarises and an AP emerges, while it fails to properly depolarise for the subcritical stimulus. The inset of Fig. 3(d) shows that the amplitude of the voltage spike undergoes a sharp step increase at the pulse strength $I = I_{\text{AP}}$, i.e. the circuit exhibits the defining all-or-none law found in biological neurons [75, 76, 81], a feature considered to be a requirement for artificial neurons [66].

For a slightly increased and sustained stimulus strength (as shown in Fig. 3(e)), the spike train of Fig. 3(f) emerges for a supercritical input $I > I_{\text{train}}$, while just a single AP appears

for a subcritical input $I < I_{\text{train}}$. Spike trains are another unique feature of neuromorphic behaviour and play a vital role in neuronal communication [76, 82–85]. In the SM [89] we show that the frequency of the spike train can be tuned by altering the capacitance and cone lengths. In Ref. [86] a spike train emerging from a simulated iontronic circuit containing quasi two-dimensional nanochannels was presented. However, the defining all-or-none law of APs [66, 75, 76, 81] was not reported in Ref. [86]. Additionally, in biological neurons the battery potentials stem from Nernst potentials, which are not considered to affect the voltage-gated channel conductances, hence $|V_i| = |V_m|$ in typical HH studies [93–100]. However, in an experimental realisation of a microfluidic HH-like circuit with electric batteries the voltages $V_i(t)$ over the channels will be affected by the battery potentials E_i , i.e. $|V_i(t)| = |V_m(t) - E_i|$. This detail is not considered in Ref. [86] and hence it is not immediately clear how this circuit could be experimentally realized.

In summary, we derived a theoretical model with no free parameters, starting from the Poisson-Nernst-Planck-Stokes equations (1)-(4), that explains how dynamic concentration polarization in conical pores facilitates a volatile conductance memory. Our theory agrees quantitatively with the memristive conductance of conical channels observed in finite-element calculations and we surprisingly find that the conductive memory retention process is governed by a slow diffusive timescale. By assembling multiple conical channels in an experimentally accessible iontronic Hodgkin-Huxley circuit we find emerging neuronal behaviour. The circuit exhibits all-or-

none action potentials upon pulse stimulation, a fundamental requirement for artificial neurons [66], and spike trains under a sustained stimulus, thereby displaying hallmark features of neuronal communication [76, 81–85]. Our work promises to accelerate the targeted development of iontronic circuits and a more effortless scanning of possible applications thereof, beyond what is presented in this Letter.

This work is part of the D-ITP consortium, a program of the Netherlands Organisation for Scientific Research (NWO) that is funded by the Dutch Ministry of Education, Culture and Science (OCW). T.M.K. performed the calculations; W.Q.B. conceptualized the work; T.M.K. and W.Q.B. developed the theory under supervision of C.S. and R.v.R. All authors discussed the results and contributed to the manuscript.

-
- [1] K. N. Knust, D. Hlushkou, U. Tallarek, and R. M. Crooks, *ChemElectroChem* **1**, 850 (2014).
- [2] S. P. Surwade, S. N. Smirnov, I. V. Vlassioug, R. R. Unocic, G. M. Veith, S. Dai, and S. M. Mahurin, *Nature Nanotechnology* **10**, 459 (2015).
- [3] C.-C. Lai, C.-J. Chang, Y.-S. Huang, W.-C. Chang, F.-G. Tseng, and Y.-L. Chueh, *Nano Energy* **12**, 394 (2015).
- [4] F. H. van der Heyden, D. J. Bonthuis, D. Stein, C. Meyer, and C. Dekker, *Nano Letters* **7**, 1022 (2007).
- [5] A. Siria, P. Poncharal, A.-L. Biance, R. Fulcrand, X. Blase, S. T. Purcell, and L. Bocquet, *Nature* **494**, 455 (2013).
- [6] K. Xiao, L. Jiang, and M. Antonietti, *Joule* **3**, 2364 (2019).
- [7] O. A. Saleh and L. L. Sohn, *Nano Letters* **3**, 37 (2003).
- [8] W. Shi, A. K. Friedman, and L. A. Baker, *Analytical Chemistry* **89**, 157 (2017).
- [9] I. Vlassioug, T. R. Kozel, and Z. S. Siwy, *Journal of the American Chemical Society* **131**, 8211 (2009).
- [10] A. De La Escosura-Muñiz and A. Merkoçi, *ACS nano* **6**, 7556 (2012).
- [11] H. Zhang, Y. Tian, and L. Jiang, *Nano Today* **11**, 61 (2016).
- [12] Z. S. Siwy, M. L. Bruening, and S. Howorka, *Chemical Society Reviews* (2023).
- [13] S. H. Han, M.-A. Oh, and T. D. Chung, *Chemical Physics Reviews* **3**, 031302 (2022).
- [14] C. Yang, K. Hu, D. Wang, Y. Zubi, S. T. Lee, P. Puthongkham, M. V. Mirkin, and B. J. Venton, *Analytical Chemistry* **91**, 4618 (2019).
- [15] K. Hu, D. Wang, M. Zhou, J. H. Bae, Y. Yu, H. Xin, and M. V. Mirkin, *Analytical Chemistry* **91**, 12935 (2019).
- [16] S. Shchanikov, A. Zuev, I. Bordanov, S. Danilin, V. Lukoyanov, D. Korolev, A. Belov, Y. Pigareva, A. Gladkov, A. Pimashkin, *et al.*, *Chaos, Solitons & Fractals* **142**, 110504 (2021).
- [17] A. Noy and S. B. Darling, *Science* **379**, 143 (2023).
- [18] C. Li, T. Xiong, P. Yu, J. Fei, and L. Mao, *ACS Applied Bio Materials* **4**, 71 (2020).
- [19] L. Jubin, A. Poggioli, A. Siria, and L. Bocquet, *Proceedings of the National Academy of Sciences* **115**, 4063 (2018).
- [20] X. Hou, W. Guo, and L. Jiang, *Chemical Society Reviews* **40**, 2385 (2011).
- [21] S. Ghosal, J. D. Sherwood, and H.-C. Chang, *Biomicrofluidics* **13**, 011301 (2019).
- [22] S. N. Bush, T. T. Volta, and C. R. Martin, *Nanomaterials* **10**, 571 (2020).
- [23] J. Liu, M. Kvetny, J. Feng, D. Wang, B. Wu, W. Brown, and G. Wang, *Langmuir* **28**, 1588 (2012).
- [24] C. Wei, A. J. Bard, and S. W. Feldberg, *Analytical Chemistry* **69**, 4627 (1997).
- [25] W. Q. Boon, T. E. Veenstra, M. Dijkstra, and R. van Roij, *Physics of Fluids* **34**, 101701 (2022).
- [26] H. S. White and A. Bund, *Langmuir* **24**, 2212 (2008).
- [27] L.-J. Cheng and L. J. Guo, *Nano Letters* **7**, 3165 (2007).
- [28] Z. S. Siwy, *Advanced Functional Materials* **16**, 735 (2006).
- [29] Z. Siwy, Y. Gu, H. Spohr, D. Baur, A. Wolf-Reber, R. Spohr, P. Apel, and Y. Korchev, *EPL (Europhysics Letters)* **60**, 349 (2002).
- [30] A. Fuliński, I. Kosińska, and Z. Siwy, *New Journal of Physics* **7**, 132 (2005).
- [31] Z. Siwy, I. Kosińska, A. Fuliński, and C. Martin, *Physical Review Letters* **94**, 048102 (2005).
- [32] D. Duleba, P. Dutta, S. Denuga, and R. P. Johnson, *ACS Measurement Science Au* (2022).
- [33] W.-J. Lan, M. A. Edwards, L. Luo, R. T. Perera, X. Wu, C. R. Martin, and H. S. White, *Accounts of Chemical Research* **49**, 2605 (2016).
- [34] I. Vlassioug, S. Smirnov, and Z. Siwy, *ACS Nano* **2**, 1589 (2008).
- [35] C. Kubeil and A. Bund, *The Journal of Physical Chemistry C* **115**, 7866 (2011).
- [36] S. Dal Cengio and I. Pagonabarraga, *The Journal of Chemical Physics* **151**, 044707 (2019).
- [37] A. R. Poggioli, A. Siria, and L. Bocquet, *The Journal of Physical Chemistry B* **123**, 1171 (2019).
- [38] Y. Uematsu, *Physics of Fluids* (2022).
- [39] M. L. Kovarik, K. Zhou, and S. C. Jacobson, *The Journal of Physical Chemistry B* **113**, 15960 (2009).
- [40] C.-Y. Lin, L.-H. Yeh, and Z. S. Siwy, *The Journal of Physical Chemistry Letters* **9**, 393 (2018).
- [41] Z. Siwy, P. Apel, D. Baur, D. D. Dobrev, Y. E. Korchev, R. Neumann, R. Spohr, C. Trautmann, and K.-O. Voss, *Surface Science* **532**, 1061 (2003).
- [42] Z. Siwy and A. Fuliński, *Physical Review Letters* **89**, 198103 (2002).
- [43] D. Wang, M. Kvetny, J. Liu, W. Brown, Y. Li, and G. Wang, *Journal of the American Chemical Society* **134**, 3651 (2012).
- [44] Y. Li, D. Wang, M. M. Kvetny, W. Brown, J. Liu, and G. Wang, *Chemical Science* **6**, 588 (2015).
- [45] D. Wang, J. Liu, M. Kvetny, Y. Li, W. Brown, and G. Wang, *Chemical Science* **5**, 1827 (2014).
- [46] D. Wang and G. Wang, *Journal of Electroanalytical Chemistry* **779**, 39 (2016).
- [47] D. Wang, W. Brown, Y. Li, M. Kvetny, J. Liu, and G. Wang, *Analytical Chemistry* **89**, 11811 (2017).
- [48] Q. Sheng, Y. Xie, J. Li, X. Wang, and J. Xue, *Chemical Communications* **53**, 6125 (2017).
- [49] W. Brown, Y. Li, R. Yang, D. Wang, M. Kvetny, H. Zheng, and G. Wang, *Chemical Science* **11**, 5950 (2020).
- [50] W. Brown, M. Kvetny, R. Yang, and G. Wang, *The Journal of Physical Chemistry C* **126**, 10872 (2022).
- [51] W. Brown, M. Kvetny, R. Yang, and G. Wang, *The Journal of Physical Chemistry C* **125**, 3269 (2021).
- [52] D. Wang, W. Brown, Y. Li, M. Kvetny, J. Liu, and G. Wang, *ChemElectroChem* **5**, 3089 (2018).
- [53] P. Ramirez, J. J. Perez-Grau, J. Cervera, S. Nasir, M. Ali, W. Ensinger, and S. Mafe, *Applied Physics Letters* **118**, 181903 (2021).
- [54] L. Chua, *IEEE Transactions on Circuit Theory* **18**, 507 (1971).

- [55] D. B. Strukov, G. S. Snider, D. R. Stewart, and R. S. Williams, *Nature* **453**, 80 (2008).
- [56] L. Chua, *Semicond. Sci. Technol.* **29**, 104001 (2014).
- [57] F. Caravelli and J. P. Carbajal, *Technologies* **6**, 118 (2018).
- [58] L. Chua, *Nanotechnology* **24**, 383001 (2013).
- [59] Y. van De Burgt, A. Melianas, S. T. Keene, G. Malliaras, and A. Salleo, *Nature Electronics* **1**, 386 (2018).
- [60] S. T. Keene, P. Gkoupidenis, and Y. Van de Burgt, in *Organic Flexible Electronics* (Elsevier, 2021) pp. 531–574.
- [61] E. Chicca and G. Indiveri, *Applied Physics Letters* **116**, 120501 (2020).
- [62] D. V. Christensen, R. Dittmann, B. Linares-Barranco, A. Sebastian, M. Le Gallo, A. Redaelli, S. Slesazek, T. Mikolajick, S. Spiga, S. Menzel, *et al.*, *Neuromorphic Computing and Engineering* **2**, 022501 (2022).
- [63] M. P. Sah, H. Kim, and L. O. Chua, *IEEE Circuits and Systems Magazine* **14**, 12 (2014).
- [64] C. D. Schuman, T. E. Potok, R. M. Patton, J. D. Birdwell, M. E. Dean, G. S. Rose, and J. S. Plank, arXiv preprint arXiv:1705.06963 (2017).
- [65] T. Venkatesan and S. Williams, *Applied Physics Reviews* **9**, 010401 (2022).
- [66] J. Zhu, T. Zhang, Y. Yang, and R. Huang, *Applied Physics Reviews* **7**, 011312 (2020).
- [67] A. Mehonic and A. J. Kenyon, *Nature* **604**, 255 (2022).
- [68] V. K. Sangwan and M. C. Hersam, *Nature Nanotechnology* **15**, 517 (2020).
- [69] F. Caravelli, F. C. Sheldon, and F. L. Traversa, *Science Advances* **7**, eabh1542 (2021).
- [70] S. T. Keene, C. Lubrano, S. Kazemzadeh, A. Melianas, Y. Tuchman, G. Polino, P. Scognamiglio, L. Cinà, A. Salleo, Y. van de Burgt, *et al.*, *Nature Materials* **19**, 969 (2020).
- [71] P. C. Harikesh, C.-Y. Yang, D. Tu, J. Y. Gerasimov, A. M. Dar, A. Armada-Moreira, M. Massetti, R. Kroon, D. Bliman, R. Olsson, *et al.*, *Nature Communications* **13**, 1 (2022).
- [72] I. Krauhausen, D. A. Koutsouras, A. Melianas, S. T. Keene, K. Lieberth, H. Ledansour, R. Sheelamanthula, A. Giovannitti, F. Torricelli, I. McCulloch, *et al.*, *Science Advances* **7**, eabl5068 (2021).
- [73] P. D. Marasco, J. S. Hebert, J. W. Sensinger, D. T. Beckler, Z. C. Thumser, A. W. Shehata, H. E. Williams, and K. R. Wilson, *Science Robotics* **6**, eabf3368 (2021).
- [74] L. Yuan, S. Liu, W. Chen, F. Fan, and G. Liu, *Advanced Electronic Materials* **7**, 2100432 (2021).
- [75] L. Squire, D. Berg, F. Bloom, S. du Lac, A. Ghosh, N. Spitzer, *Fundamental Neuroscience*, 3rd ed. (Academic Press, 2008) Chap. 11.
- [76] B. P. Bean, *Nature Reviews Neuroscience* **8**, 451 (2007).
- [77] T. Xiong, C. Li, X. He, B. Xie, J. Zong, Y. Jiang, W. Ma, F. Wu, J. Fei, P. Yu, *et al.*, *Science* **379**, 156 (2023).
- [78] P. Robin, T. Emmerich, A. Ismail, A. Niguès, Y. You, G.-H. Nam, A. Keerthi, A. Siria, A. Geim, B. Radha, *et al.*, *Science* **379**, 161 (2023).
- [79] B. Xie, T. Xiong, W. Li, T. Gao, J. Zong, Y. Liu, and P. Yu, *Chemistry—An Asian Journal* **17**, e202200682 (2022).
- [80] D. Kim and J.-S. Lee, *ACS Applied Electronic Materials* (2023).
- [81] K. Lucas, *The Journal of Physiology* **38**, 113 (1909).
- [82] L. Squire, D. Berg, F. Bloom, S. du Lac, A. Ghosh, N. Spitzer, *Fundamental Neuroscience*, 3rd ed. (Academic Press, 2008) Chap. 6.
- [83] G. S. Cymbalyuk, Q. Gaudry, M. A. Masino, and R. L. Calabrese, *Journal of Neuroscience* **22**, 10580 (2002).
- [84] E. Marder and V. Thirumalai, *Neural Networks* **15**, 479 (2002).
- [85] S. M. Sherman, *Trends in Neurosciences* **24**, 122 (2001).
- [86] P. Robin, N. Kavokine, and L. Bocquet, *Science* **373**, 687 (2021).
- [87] B. J. Kirby and E. F. Hasselbrink Jr, *Electrophoresis* **25**, 187 (2004).
- [88] M. Aarts, W. Q. Boon, B. Cuénod, M. Dijkstra, R. van Roij, and E. Alarcon-Llado, *ACS Applied Materials & Interfaces* (2022).
- [89] See Supplemental Material for the derivation of Eq. (6), a discussion of the range of validity of the analytical approximation and an analysis of the circuit as a dynamical system, which includes Refs. [102–108].
- [90] V. S. Markin, A. G. Volkov, and L. Chua, *Plant signaling & behavior* **9**, e972887 (2014).
- [91] C. Multiphysics, COMSOL Multiphysics, Burlington, MA, accessed Feb **9**, 32 (1998).
- [92] R. W. Pryor, *Multiphysics modeling using COMSOL®: a first principles approach* (Jones & Bartlett Publishers, 2009).
- [93] A. L. Hodgkin and A. F. Huxley, *The Journal of Physiology* **117**, 500 (1952).
- [94] W. Rall, *Comprehensive Physiology*, 39 (2011).
- [95] R. FitzHugh, *Journal of Theoretical Biology* **40**, 517 (1973).
- [96] W. Rall, *Annals of the New York Academy of Sciences* **96**, 1071 (1962).
- [97] J. A. Halter and J. Clark Jr, *Journal of Theoretical Biology* **148**, 345 (1991).
- [98] E. Hay, S. Hill, F. Schürmann, H. Markram, and I. Segev, *PLOS Computational Biology* **7**, e1002107 (2011).
- [99] M. L. Hines and N. T. Carnevale, *Neural Computation* **9**, 1179 (1997).
- [100] M. H. Kole, S. U. Ilshner, B. M. Kampa, S. R. Williams, P. C. Ruben, and G. J. Stuart, *Nature Neuroscience* **11**, 178 (2008).
- [101] L. J. Gentet, G. J. Stuart, and J. D. Clements, *Biophysical Journal* **79**, 314 (2000).
- [102] R. FitzHugh, *Biophysical Journal* **1**, 445 (1961).
- [103] J. Nagumo, S. Arimoto, and S. Yoshizawa, *Proceedings of the IRE* **50**, 2061 (1962).
- [104] J. Bisquert, *The Journal of Physical Chemistry Letters* **12**, 11005 (2021).
- [105] W. C. Troy, *Journal of Mathematical Analysis and Applications* **54**, 678 (1976).
- [106] A. Rabinovitch and I. Rogachevskii, *Chaos: An Interdisciplinary Journal of Nonlinear Science* **9**, 880 (1999).
- [107] J. K. Hale and H. Koçak, *Dynamics and Bifurcations*, Vol. 3 (Springer Science & Business Media, 2012) Chap. 11.
- [108] S. Lynch, *Dynamical Systems with Applications using MATLAB* (Springer, 2004) Chap. 13.

Supplemental Material for “Iontronic neuromorphic signalling with conical microfluidic memristors”

T. M. Kamsma,^{1,2} W. Q. Boon,¹ T. ter Rele,^{1,3} C. Spitoni,² and R. van Roij¹

¹*Institute for Theoretical Physics, Utrecht University, Princetonplein 5, 3584 CC Utrecht, The Netherlands*

²*Mathematical Institute, Utrecht University, Budapestlaan 6, 3584 CD Utrecht, The Netherlands*

³*Soft Condensed Matter, Debye Institute for Nanomaterials Science, Utrecht University, Princetonplein 1, 3584 CC Utrecht, The Netherlands*

I. CHANNEL MEMORY TIMESCALE AND RANGE OF VALIDITY

To derive the memory retention timescale τ of a conical channel from the PNPS equations, we consider two quantities, the change of total number of ions in the channel and the net salt flux. The total number of ions in the channel $N = \pi \int_0^L R^2(x) \bar{\rho}_s(x, V) dx$ changes when a voltage is applied over the channel. Using results from Ref. [1] for the radially averaged steady-state salt concentration at a static voltage V ,

$$\bar{\rho}_s(x, V) = 2\rho_b + 2\rho_b \Delta g \left[\frac{x}{L} \frac{R_t}{R(x)} - \frac{e^{\frac{Pe(V)}{L} \frac{R_t^2}{R_b R(x)}} - 1}{e^{\frac{Pe(V)}{L} \frac{R_t^2}{R_b}} - 1} \right], \quad (S1)$$

we find that the change in N upon a small voltage perturbation V' around $V = 0$ yields

$$\begin{aligned} \frac{\partial N}{\partial V} \Big|_{V=0} V' &= \left(\pi \int_0^L R^2(x) \frac{\partial \bar{\rho}_s(x, V)}{\partial V} dx \right) V' \\ &= \frac{\pi}{6} L \Delta R \frac{e\sigma}{k_B T} V' \equiv \alpha V', \end{aligned} \quad (S2)$$

where $\alpha < 0$ for our parameter choice of $\sigma < 0$ and $\Delta R > 0$, in agreement with the enhanced (reduced) conductance of a negative (positive) potential V' .

We can find the time it takes to add $\alpha V'$ ions to the channel by considering the salt current J . For the net total influx of salt into the channel due to a change in the static electric potential we use the expression for the total salt flux, i.e. the x -component of J , given in Ref. [1] by

$$\begin{aligned} J_x(x) &= -D \left(\pi R^2(x) \partial_x \bar{\rho}_s(x, V) + 2\pi\sigma \frac{eV}{k_B T} \frac{R_t R_b}{R(x)L} \right) \\ &\quad + Q(V) \bar{\rho}_s(x, V) \end{aligned} \quad (S3)$$

which represents the diffusive, conductive and advective components, respectively and where $Q(V) = -\frac{V}{L} \pi R_t R_b \frac{\epsilon \psi_0}{\eta}$ is the electro-osmotic volume flow. The net total number of ions entering the channels is given by the difference in salt flux between the tip and base $J_x(L) - J_x(0)$. Since we consider a small voltage perturbation V' around $V = 0$, we consider an initially homogeneous state $\bar{\rho}_s(x) = 2\rho_b$ where $\partial_x \bar{\rho}_s(x, V) = 0$. In this case the first term in Eq. (S3) vanishes and also the third term vanishes as Q is laterally constant and $\bar{\rho}_s(0, V) = \bar{\rho}_s(L, V)$. The resulting net salt flux at a small static potential V' is then purely given by the conductive terms

$$J_x(0) - J_x(L) = 2\pi \frac{D \Delta R}{L} \frac{e\sigma}{k_B T} V' \equiv \gamma V', \quad (S4)$$

where $\gamma < 0$ for our parameter choice of $\sigma < 0$ and $\Delta R > 0$. With α and γ defined in Eqs. (S2) and (S4), respectively, we obtain the timescale τ of interest as

$$\tau = \frac{\alpha}{\gamma} = \frac{1}{12} \frac{L^2}{D}, \quad (S5)$$

via which we see that the timescale is dictated by the characteristic diffusion time of the channel. This is a surprising result as the $\gamma V'$ of Eq. S3 term is purely conductive. Eq. (S5) is plotted in the right inset of Fig. 2, where we compare τ with the reciprocal frequencies $1/f_{\max}$ from full finite-element for which the enclosed area in the I-V hysteresis loop is maximal for various lengths, for all L they are related via $f_{\max} \tau \approx 0.19$.

To arrive at Eq. (S4), through which Eq. (S1) is obtained in Ref. [1], the assumption is made that $\lambda_D \ll R(x)$, which we mildly violate around the tip of the channel for our standard parameter set. Nevertheless, we still obtain good agreement with finite element calculations, however we note that our analytical approximation is not necessarily universally applicable to all parameter sets. We remark that in our work the emergence of neuromorphic behaviour was rather sensitive to changes in the parameters. Although we obtained spiking for numerous different parameter sets, this sensitivity suggests that explorations of the parameter space would be required in experiments.

II. EXPLANATION OF SPIKE TRAIN AND FREQUENCY MODULATION

Eqs. (7) and (9) form a dynamical system of equations, which we can analyse in some more detail to gain a deeper understanding of the spiking behaviour presented in Fig. 3. Firstly, since $\tau_{\pm} \ll \tau_s$ we can assume instantaneity of the g_{\pm} channels, i.e. $g_{\pm}(V(t), t) = g_{\infty, \pm}(V(t))$. With this assumption the current contribution in the circuit in Fig. 3(b) through the fast channels is determined directly by Eq. (5), i.e.

$$\begin{aligned} g_r F(V_m(t)) &\equiv -g_{\infty, +}(-V_m(t) + E_+) (V_m(t) - E_+) \\ &\quad - g_{\infty, -} (V_m(t) - E_-) (V_m(t) - E_-), \end{aligned} \quad (S6)$$

representing the total current from the fast channels and which we denote by $g_r F(V_m(t))$ where g_r is a characteristic effective conductance of the fast channels. By expanding Eq. (S6) in $V_m(t)$, we find that $F(V_m(t))$ is well-approximated by

$$g_r F(V_m(t)) \approx \mathcal{G} V_m(t) - \frac{(\mathcal{G} V_m(t))^3}{3V_r^2}, \quad (S7)$$

where the characteristic effective conductance of the fast channels $g_r = 1$ pS, a reference voltage $V_r = 1$ V and a dimensionless parameter $\mathcal{G} = 3.5$ are determined by expanding $F(V_m(t))$ around $V_m(t) = 0$.

This assumption reduces the dynamical system to a set of only two ordinary differential equations, given by

$$\tau_m \frac{dV_m(t)}{dt} = \frac{I(t)}{g_r} - \frac{g_s(t)}{g_r} (V_m(t) - E_s) + F(V_m(t)), \quad (\text{S8})$$

$$\tau_s \frac{dg_s(t)}{dt} = g_{\infty,s}(-V_m(t) + E_s) - g_s(t), \quad (\text{S9})$$

where we defined a membrane response RC time of $\tau_m = C/g_r = 5$ ms, for the parameter set used in Fig. 3. With Eqs. (S8) and (S9) we obtain results that are essentially indistinguishable from those in Fig. 3.

Eqs. (S8) and (S9) suggest that it is possible to modulate the spike train frequency by altering the two timescales τ_m and τ_s . Physically this could be achieved by tuning the capacitance C and the slow channel length L_s , respectively. If we scale both τ_m and τ_s by the same factor n^* , i.e. $\tau_m \rightarrow n^* \tau_m$ and $\tau_s \rightarrow n^* \tau_s$, we indeed see in Fig. S1 that the spike train period depends essentially linearly on this factor n^* , where we again solved the full system of Eqs. (7) and (9).

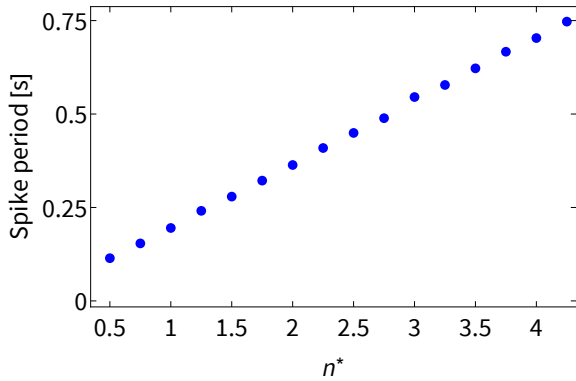


Figure S1. The spike train period from the circuit presented in Fig. 3(b) as a result of the full system of Eqs. (7) and (9) when the timescales τ_m and τ_s are rescaled by a factor n^* , i.e. $\tau_m \rightarrow n^* \tau_m$ and $\tau_s \rightarrow n^* \tau_s$.

We observe that Eqs. (S8) and (S9) are very similar to the FitzHugh-Nagumo (FN) model (also known as the Bonhoeffer-van der Pol model), which is of no surprise since these models serve as simplified versions of the HH model [2, 3]. In particular, Eqs. (S8) and (S9) are formulated similar to the system investigated in Ref. [4]. Although the FN model is not identical to Eqs. (S8) and (S9), we do believe that both the all-or-none behaviour and the spike train behaviour can be understood through the FN model, an approach that was used to understand the original HH model results as well [2–6].

A mathematical understanding of the spiking behaviour through the FN model has been broadly investigated [2–6]. Additionally we offer here a heuristic explanation of why we see emerging neuromorphic behaviour from our specific ionic circuit. If we consider the circuit in Fig. 3(b) without

the slow channel and with $I(t) = 0$, then we find two stable stationary points at $V_m \approx \pm 0.5$ V. These stationary points correspond to the non-trivial roots of $F(V_m)$. This bistability is a precursor of the all-or-none law we find. For a sufficiently

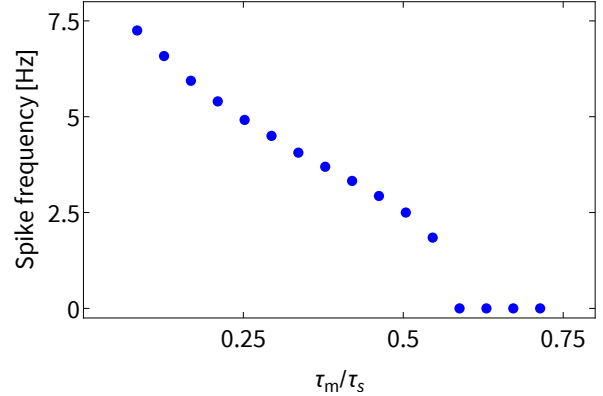


Figure S2. The spike train frequency from the circuit presented in Fig. 3(b) as a result of the full system of Eqs. (7) and (9) when the timescales τ_m is changed while τ_s is kept constant. The spike train only emerges if $\tau_m < 0.55 \tau_s$.

strong imposed stimulus current $I(t) = I > 0$, the negative stationary state vanishes and only a positive stable stationary state $V_m > 0$ remains. The $V_m < 0$ state for $I(t) = 0$ also emerges in the full circuit with the slow channel (Fig. 3(b)), which we observe as the initial resting state as seen in Figs. 3(d) and 3(f). A $V_m > 0$ state is not present here because the slow channel becomes more conductive for $V_m > 0$ and pushes $V_m(t)$ to the battery potential $E_s < 0$. Now assume the full system is at rest with $I(t) = 0$ at $V_m(t) = V_m^* < 0$ and we increase $I(t)$ at time t' from 0 to some $I > I_{AP}$. Then after some time $\Delta t \ll \tau_s$, such that $g_s(t' + \Delta t) \approx g_s(t') = g_{\infty,s}(V_m^*)$, the slow channel is still in a low conducting state. If $V_m(t)$ is able to significantly change over a time period Δt , then the system can transition to the $V_m > 0$ stationary state before the slow channel becomes conductive enough to make this state vanish. Note that this requires that the RC-like membrane voltage response time τ_m is much shorter than the slow channel timescale, i.e. $\tau_m \ll \tau_s$. In Fig. S2, which shows the spike train frequency as a function of τ_m/τ_s , we show that this requirement actually also holds for the full circuit presented in Fig. 3(b). A spike train only emerges when $\tau_m < 0.55 \tau_s$ and for $\tau_m > 0.55 \tau_s$ the spike train does not emerge, corresponding to a frequency of 0 in Fig. S2. This fast-slow relation is characteristic for FN models [2] and this requirement is also found in Ref. [4].

The all-or-none behaviour can now be explained by the observation that the $V_m < 0$ stationary state either remains in place for $I < I_{AP}$ (thus no action potential) or vanishes temporarily for $I > I_{AP}$, resulting in a complete action potential. For a stimulus current $I_{AP} < I < I_{train} \approx 1.28$ pA there is still a stable stationary point, which can be seen in the subcritical voltage trace in Fig. 3(f, red). At $I = I_{train} \approx 1.28$ pA, this stable point undergoes a Hopf bifurcation [7] and the trace

shows a periodic solution, as shown in Fig. 3(f, blue). After the Hopf bifurcation two more stationary points appear inside the stable limit cycle which are both also unstable, thus it is a supercritical Hopf bifurcation [8].

With the identification that the relevant dynamical variables are $V_m(t)$ and $g_s(t)$ we can alternatively display the results from Figs. 3(d) and 3(f) in a phase portrait of $V_m(t)$ and $g_s(t)$. In Fig. S3 we show the trajectories of $V_m(t)$ and $g_s(t)$ which start out from a resting state with $I = 0$, after which sustained currents of $I = 1.16 \text{ pA} < I_{AP}$, $I_{AP} < I = 1.27 \text{ pA} < I_{train}$ and $I = 1.28 \text{ pA} > I_{train}$ are imposed, resulting in the green, red and blue trajectories, respectively. The green trajectory settles to a new stationary state rather directly, while the red trajectory first traverses a single orbit through the $(V_m(t), g_s(t))$ space, which is visible as the single action potential shown in Fig. 3(d). The supercritical Hopf bifurcation at $I = 1.28 \text{ pA}$ translates to the blue periodic orbit, corresponding to the spike train shown in Fig. 3(f).

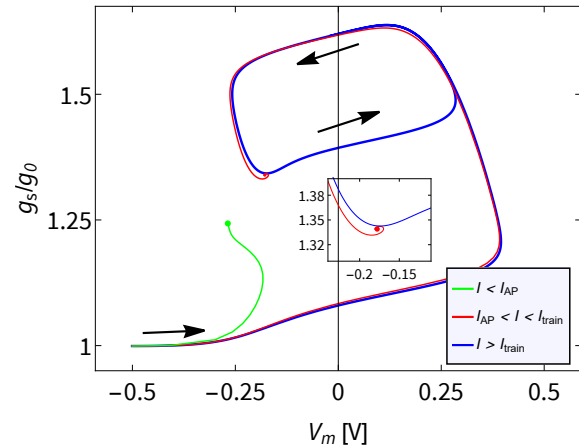


Figure S3. The phase portrait of $V_m(t)$ and $g_s(t)$, obtained by solving the two-dimensional set of equations (S8) and (S9). The trajectories of $V_m(t)$ and $g_s(t)$ start out from a resting state with $I = 0$, after which sustained currents of $I = 1.16 \text{ pA} < I_{AP}$, $I_{AP} < I = 1.27 \text{ pA} < I_{train}$ and $I = 1.28 \text{ pA} > I_{train}$ resulting in the green, red and blue trajectories, respectively.

[1] W. Q. Boon, T. E. Veenstra, M. Dijkstra, and R. van Roij, *Physics of Fluids* **34**, 101701 (2022).
 [2] R. FitzHugh, *Biophysical Journal* **1**, 445 (1961).
 [3] J. Nagumo, S. Arimoto, and S. Yoshizawa, *Proceedings of the IRE* **50**, 2061 (1962).
 [4] J. Bisquert, *The Journal of Physical Chemistry Letters* **12**, 11005 (2021).
 [5] W. C. Troy, *Journal of Mathematical Analysis and Applications*

54, 678 (1976).
 [6] A. Rabinovitch and I. Rogachevskii, *Chaos: An Interdisciplinary Journal of Nonlinear Science* **9**, 880 (1999).
 [7] J. K. Hale and H. Koçak, *Dynamics and Bifurcations*, Vol. 3 (Springer Science & Business Media, 2012) Chap. 11.
 [8] S. Lynch, *Dynamical Systems with Applications using MATLAB* (Springer, 2004) Chap. 13.